

Production, structure, and optical properties of ZnO nanocrystals embedded in CaF₂ matrix

Y. C. Liu^{a)}

Key Laboratory of Excited State Processes, Chinese Academy of Sciences, Changchun Institute of Optics, Fine Mechanics and Physics, Chinese Academy of Sciences, 140 Renmin Street, Changchun 130021, People's Republic of China

H. Y. Xu

Advanced Center for Opto-electronic Functional Material Research, Northeast Normal University, 138 Renmin Street, Changchun 130024, People's Republic of China

R. Mu and D. O. Henderson

Chemical Physics Laboratory, Department of Physics, Fisk University, Nashville, Tennessee 37028

Y. M. Lu, J. Y. Zhang, D. Z. Shen, and X. W. Fan

Key Laboratory of Excited State Processes, Chinese Academy of Sciences, Changchun Institute of Optics, Fine Mechanics and Physics, Chinese Academy of Sciences, 140 Renmin Street, Changchun 130021, People's Republic of China

C. W. White

Oak Ridge National Laboratory, Oak Ridge, Tennessee 37831

(Received 16 January 2003; accepted 13 May 2003)

High-quality ZnO nanocrystals have been fabricated by zinc ion implantation (160 keV, 1×10^{17} ions/cm²) into a CaF₂(111) single-crystal substrate followed by thermal annealing from 300 to 700 °C. X-ray diffraction results show that ZnO nanocrystals in CaF₂(111) substrate have a (002) preferred orientation. The average grain size is ranging from 14 to 19 nm corresponding to the annealing temperatures from 500 to 700 °C. A very strong ultraviolet near-band edge emission is observed from 372 to 379 nm. The emission intensity is enhanced and linewidth is narrowed as the annealing temperature increases. The commonly observed visible green emission associated with deep-level defects in ZnO is suppressed. © 2003 American Institute of Physics.

[DOI: 10.1063/1.1591248]

ZnO is a versatile wide band gap (3.3 eV) semiconducting material with a large exciton binding energy of 60 meV at RT. Recently, it has gained even more interest in the application of optoelectronic devices due to the discovery of low-voltage electroluminescence¹ and UV lasing effects.² A recent report showed that the homoepitaxial N-doped *p*-type ZnO was produced by molecular beam epitaxy (MBE) suggesting that a *p*-*n* homojunction device is possible.³ ZnO nanocrystals embedded in solid matrix are used to fabricate quantum dots that can lead to further enhancement of light emission intensity due to the zero-dimensional quantum confinement effects of both electrons and holes. The quantum confinement can also reveal other unique optical properties, which are not observed in its bulk. High quality ZnO films can be prepared by many methods such as sputtering,⁴ pulse laser deposition,⁵ chemical vapor deposition,⁶ the oxidation of metallic Zn,⁷ and molecular beam epitaxy.⁸ However, ZnO nanocrystals embedded in solid matrix are difficult to fabricate by aforementioned techniques. Thus, ion implantation was the purpose of the choice. In addition, ion implantation is the cleanest and versatile technique to obtain nanocrystals in the near surface for a wide variety of materials.⁹ This

method has been used to fabricate Si, Ge, GaAs, and GaN nanocrystals embedded in SiO₂ and Al₂O₃, just to name a few.¹⁰⁻¹³

In this letter, we report on the formation of ZnO nanocrystals in CaF₂ substrate via Zn ion implantation followed by thermal annealing. X-ray diffraction (XRD), microphotoluminescence (μ -PL), and absorption spectra were used to characterize the formation and quality of ZnO nanocrystals. This reports on the ZnO nanocrystals formation in CaF₂ with (002) preferred orientation synthesized by ion implantation and thermal annealing processes.

The motivation to choose CaF₂ single crystal as a host material was that CaF₂ is (1) a highly transparent wide-band gap material (11.8 eV at 298 K),¹⁴ (2) chemically stable, and (3) a low refractive index material with the indices of 1.3 and 2.4 for CaF₂ and ZnO in the UV region. Thus, it is possible to form a waveguide structure of air/ZnO/CaF₂. The exciton luminescence of ZnO nanocrystals embedded in CaF₂ can be effectively confined in the ZnO thin layer.

Highly transparent CaF₂(111) single crystal was used as a substrate. Zn ions with the energy of 160 keV were injected into the CaF₂ matrix. The dose of implanted Zn was 1×10^{17} ions/cm². Based on Rutherford backscattering measurement and TRIM simulation, the Zn ion distribution in the CaF₂ forms a nearly Gaussian shape. The ion density maximum was located 94 ± 10 nm below the surface. The samples were annealed in a furnace at temperatures from 300 to

^{a)}Author to whom correspondence should be addressed; also at: Advanced Center for Opto-electronic Functional Material Research, Northeast Normal University, 138 Renmin Street, Changchun 130024, People's Republic of China; electronic mail: ycliu@nenu.edu.cn

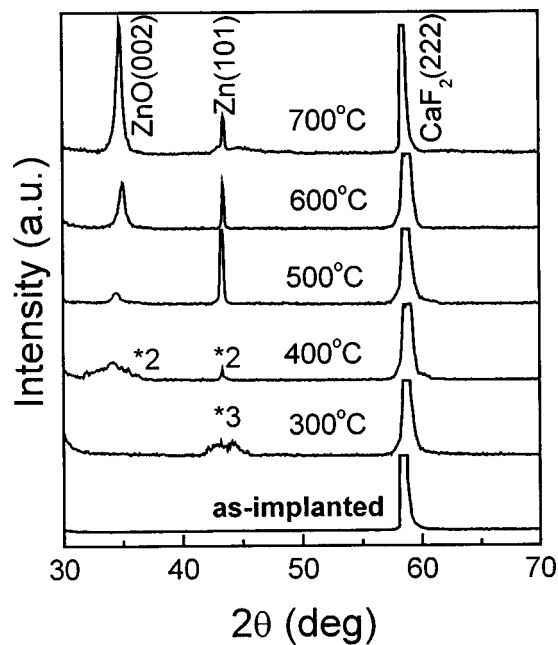


FIG. 1. XRD spectra of as-implanted sample and ZnO nanocrystals embedded in CaF_2 at different annealing temperatures.

700 °C in oxygen for 45 min. X-ray diffraction spectra were measured by D/max-rA Rigoku x-ray diffractometer with a $\text{Cu } K\alpha$ line of 1.540 56 Å. Optical absorption spectra were obtained by an UV 360 spectrophotometer (Shimadzu) at room temperature. μ -PL measurements were conducted with a J-Y UV-lamb micro-Raman spectrometer in backscattering configuration. All μ -PL spectra were obtained at RT. A 325 nm line of a He-Cd laser was used as the excitation source.

Figure 1 shows XRD traces (θ - 2θ) of as-implanted sample and ZnO nanocrystals embedded in CaF_2 at the annealing temperatures from 300 to 700 °C. For the as-implanted sample, there were no diffraction peaks detectable that were related to either metallic Zn or ZnO nanocrystals. This suggests that the majority of the implanted Zn ions were well dispersed in the implanted layer and no appreciable amount of Zn nanocrystals were formed. After the sample was annealed at 300 °C, only a broad diffraction peak of metallic Zn with a (101) orientation was observed at $\sim 43.3^\circ$ indicating that the dispersed metallic Zn started to form the Zn nanocrystals with (101) orientation. When the sample was annealed from 400 to 700 °C, the XRD diffraction peaks showed coexisting spectra of both Zn and ZnO nanocrystals diffraction peaks illustrating an interplay between the Zn and ZnO nanocrystals formation. While the formation of Zn nanocrystals occurs through thermal diffusion, ZnO nanocrystal formation may be arguably due to the metallic nanocrystal oxidation. The formed ZnO nanocrystals had a preferred (002) orientation. As the annealing temperature reached 700 °C, most of the Zn nanocrystals were oxidized into ZnO nanocrystals, but a trace of the Zn nanocrystals was still detectable based on the XRD spectrum. It is known that the peak position of (002) orientation for bulk crystals should be at $2\theta = 34.42^\circ$.¹⁵ However, the measured diffraction peak (002) of ZnO nanocrystals from this experiment was located $\sim 34.4^\circ$ - 35.0° . The slight shift with respect to the bulk value may suggest a slight decrease in lattice constant parallel to c axis of ZnO nanocrystals. This may be attributed to the stress

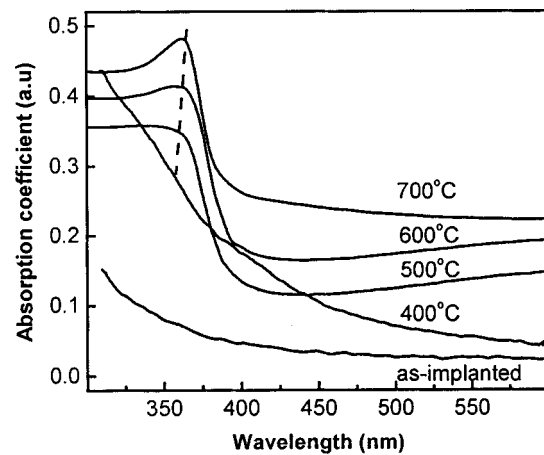


FIG. 2. Absorption spectra of as-implanted sample and ZnO nanocrystals embedded in CaF_2 at different annealing temperatures.

from CaF_2 matrix. In order to evaluate the mean grain size of ZnO nanocrystals, the Scherrer formula¹⁶ was used

$$D = \frac{0.9\lambda}{B \cos(\theta_B)},$$

where λ , θ_B , and B are the x-ray wavelength (1.540 56 Å), Bragg diffraction angle and the full width at half maximum (FWHM) of (002) diffraction peak around 34.42° , respectively. The calculated grain sizes of ZnO nanocrystals were 14, 16, and 19 nm for annealing temperatures of 500, 600, and 700 °C, respectively. As expected, the average particle size increased with the increase of annealing temperatures.

Figure 2 shows the absorption spectra of as-implanted and annealed samples at different temperatures. When the annealing temperature was below 500 °C, the observed broad and featureless absorption was primarily due to the ion beam damage to the host material, which masked the relatively weak absorption of Zn and ZnO species and clusters. The absorption due to ion beam damage is attributed to the F centers (an electron trapped at a fluorine vacancy) created in the CaF_2 single crystal. When the temperature increased, some of the F centers was annealed out via thermally assisted diffusion of displaced F ions refilled the F centers. As discussed later, F-center diffusion was also occurred to form F-center clusters— F_n centers. The exciton absorption peak at 353 nm started to appear when the annealing temperature increased to 500 °C. The absorption peak intensity was further enhanced with a slight redshift as the temperature further increased. Qualitatively, the weakening of quantum confinement effect may explain the redshift of the exciton absorption peak. The observation of the distinct exciton absorption feature in the ZnO nanocrystals embedded in CaF_2 is attributed to the large exciton binding energy of ZnO itself ~ 60 meV.

Figure 3 shows the RT PL spectra of the as-implanted sample and the ZnO nanocrystals embedded in CaF_2 which were annealed at different temperatures. For the as-implanted sample, two emissions could be detected located at ~ 340 and ~ 418 nm, although they were very weak. The two bands could be assigned to F and F_n centers and to a possible Zn ion replaced Ca ion sites.^{17,18} Certainly, the emission at ~ 340 nm may also be due to the unidentified trace level

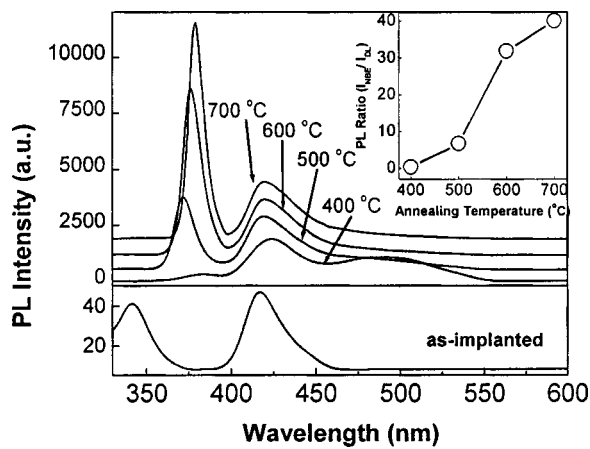


FIG. 3. Room temperature PL spectra of as-implanted sample and ZnO nanocrystals embedded in CaF_2 at different annealing temperatures. The inset shows the intensity ratio of the UV near-band edge emission to the deep level emission for the samples annealed at different temperatures.

impurities present in the as-received wafer. While the emission at ~ 418 nm was argued to be the results of F_n center formation at higher temperature. An article was planned to submit soon that is primarily focused on the defects related emission. An additional UV emission band at 384 nm with a broad linewidth was also observed at the annealing temperature at 400 °C together with another band at ~ 500 nm. These two emissions were attributed to ZnO nanocrystals formed in the host as the results of thermal annealing and oxidation. The former was due to free and bound exciton emission while the later was attributed to deep level and surface defect emissions of the ZnO nanocrystals. When the annealing temperature was above 500 °C, a strong UV emission was observed. As the annealing temperature increased from 400 to 700 °C, the UV emission peak intensity further increased, the linewidth narrowed, and the peak position redshifted from 372 to 379 nm. The measured the FWHM were 207, 125, 110, and 91 meV, respectively for the samples annealed at 400, 500, 600, and 700 °C.

On the other hand, the intensity of the emission at ~ 500 nm was decreased quickly as the annealing temperature increased. When the sample was annealed at 700 °C, the deep-level emission was almost quenched similar to the study of a polycrystalline ZnO thin film prepared by the oxidation of the metallic Zn.⁷ One way to evaluate the concentration of structural defects in ZnO nanocrystals is to compare the PL intensity ratio of the UV emission to the deep level green emission. In our experiment, the largest ratio is 41 at RT (see inset in Fig. 3), compared with the 20 observed for MBE-grown ZnO films at RT.⁸ These indicate the concentrations of the defects responsible for the deep level emission are relatively low.

Because the exciton binding energy of ZnO is about 60 meV, exciton emission can be observed at RT. In the PL spectra in Fig. 3, Exciton emission peak was redshifted ~ 62 meV to the low energy side with an increase of grain size from 14 to 19 nm corresponding to the annealing temperature from 500 to 700 °C. The particle size dependence on the

shift of the exciton emission peak is expected to be mainly due to a quantum-confinement-induced energy gap enhancement.

In conclusion, we have synthesized ZnO nanocrystals embedded in CaF_2 matrix with (002) preferential orientation by the thermal annealing the Zn ion implanted into CaF_2 substrate in oxygen ambient. XRD results show the Zn metal starts to be oxidized at 400 °C annealing temperature. As the annealing temperature increases from 500 to 700 °C, the following effects are observed: (1) the grain size increases from 14 to 19 nm, (2) the PL spectra at RT show the UV emission intensity increases and the deep-level green emission decreases (for the sample annealed at 700 °C, (3) the deep-level emission is almost quenched), (4) the UV emission peak position has a redshift from 372 to 379 nm due to the quantum confinement effect and stress effect, and (5) its FWHM decreases from 207 to 91 meV, compared with the 98 meV observed for ZnO epilayers grown on CaF_2 by MBE. These results indicate the high-quality ZnO nanocrystals embedded in CaF_2 are formed.

This work is supported by the Program of CAS Hundred Talents, the National Natural Science Foundation of China No. 60176003, the Excellent Young Teacher Foundation of Ministry of Education of China, and the Excellent researcher to go beyond century of Ministry of Education of China.

- ¹P. H. Holloway, T. A. Trottier, B. Abrams, C. Kondoleon, S. L. Jones, J. S. Sebastian, W. J. Thomas, and H. Swart, *J. Vac. Sci. Technol. B* **17**, 758 (1999).
- ²H. Cao, J. Y. Xu, E. W. Seeling, and R. P. H. Chang, *Appl. Phys. Lett.* **76**, 2997 (2000); *Phys. Rev. Lett.* **84**, 5584 (2000).
- ³D. C. Look, D. C. Reynolds, C. W. Litton, R. L. Jones, D. B. Eason, and G. Cantwell, *Appl. Phys. Lett.* **81**, 1830 (2002).
- ⁴K. K. Kim, J. H. Song, H. J. Jung, and S. J. Park, *J. Appl. Phys.* **87**, 3573 (2000).
- ⁵Y. R. Ryu, S. Zhu, J. D. Budai, H. R. Chandrasekhar, P. F. Miceli, and H. W. White, *J. Appl. Phys.* **88**, 201 (2000).
- ⁶A. Gulino, F. Castelli, P. Rossi, and I. Fragala, *Chem. Mater.* **12**, 548 (2000).
- ⁷S. Cho, J. Ma, Y. Kim, Y. Sun, G. K. L. Wong, and J. B. Ketterson, *Appl. Phys. Lett.* **75**, 2761 (1999).
- ⁸Y. Chen, D. M. Bagnall, H. J. Koh, K. T. Park, K. Hiraga, Z. Zhu, and T. Yao, *J. Appl. Phys.* **84**, 3912 (1998).
- ⁹R. Mu, D. O. Henderson, Y. S. Tung, A. Ueda, C. Hall, W. E. Collins, C. W. White, R. A. Zuhr, and J. G. Zhu, *J. Vac. Sci. Technol. A* **14**, 1482 (1996).
- ¹⁰J. G. Zhu, C. W. White, J. D. Budai, S. P. Withrow, and Y. Chen, *J. Appl. Phys.* **78**, 4386 (1995).
- ¹¹C. W. White, J. D. Budai, S. P. Withrow, S. J. Pennycook, D. M. Hembree, Jr., D. S. Zhou, T. Vo-Dinh, and R. H. Magruder, *Mater. Res. Soc. Symp. Proc.* **316**, 487 (1994).
- ¹²C. W. White, J. D. Budai, J. G. Zhu, S. P. Withrow, R. A. Zuhr, D. M. Hembree, A. Ueda, Y. S. Tung, R. Mu, and R. H. Magruder, *J. Appl. Phys.* **79**, 1876 (1996).
- ¹³J. A. Wolk, K. M. Yu, E. D. Bourret-Courchesne, and E. Johnson, *Appl. Phys. Lett.* **70**, 2268 (1997).
- ¹⁴T. Tsujibayashi, K. Toyoda, S. Sakuragi, M. Kamada, and M. Kamada, *Appl. Phys. Lett.* **80**, 2883 (2002).
- ¹⁵V. Gupta and A. Mansingh, *J. Appl. Phys.* **80**, 1063 (1996).
- ¹⁶B. D. Cullity, *Elements of X-Ray of Diffractions* (Addition-Wesley, Reading, MA, 1978), p. 102
- ¹⁷D. L. Staebler and S. E. Schnatterly, *Phys. Rev. B* **3**, 516 (1971).
- ¹⁸M. Mizuguchi, H. Hosono, H. Kawazoe, and T. Ogawa, *Proc. SPIE* **3424**, 60 (1998).